

## LENSING AND THE CENTERS OF DISTANT EARLY-TYPE GALAXIES

CHARLES R. KEETON<sup>1</sup>

Astronomy and Astrophysics Department, University of Chicago, 5640 S. Ellis Ave., Chicago, IL 60637

*Submitted to The Astrophysical Journal*

### ABSTRACT

Gravitational lensing provides a unique probe of the inner 10–1000 pc of distant galaxies ( $z \sim 0.2$ –1). Lens theory predicts that every strong lens system should have a faint image near the center of the lens galaxy, which should be visible in radio lenses but have not been observed. We study these “core” images using models derived from the stellar distributions in nearby early-type galaxies. We find that realistic galaxies predict a remarkably wide range of core images, with lensing magnifications spanning some six orders of magnitude. More concentrated galaxies produce fainter core images, although not with any simple, quantitative, model independent relation. Some real galaxies have diffuse cores and predict bright core images (magnification  $\mu_{\text{core}} \gtrsim 0.1$ ), but more common are galaxies that predict faint core images ( $\mu_{\text{core}} \lesssim 0.001$ ). Thus, stellar mass distributions alone are probably concentrated enough to explain the lack of observed core images, and may require observational sensitivity to improve by an order of magnitude before detections of core images become common. Two-image lenses will tend to have brighter core images than four-image lenses, so they will be the better targets for finding core images and exploiting these tools for studying the central mass distributions of distant galaxies.

*Subject headings:* galaxies: elliptical and lenticular, cD — galaxies: nuclei — galaxies: structure — gravitational lensing

### 1. INTRODUCTION

Galaxy centers are interesting places to study dynamics and galaxy formation. Their short crossing times make them sensitive to dynamical processes such as relaxation and binary black hole heating (e.g., Ebisuzaki, Makino & Okumura 1991; Milosavljevic & Merritt 2001). Their deep potential wells collect remnants of the galaxy formation process such as the cores of accreted galaxies (e.g., de Zeeuw & Franx 1991; Barnes & Hernquist 1992). Their dark matter content provides clues to the interaction between baryons and dark matter by adiabatic compression during galaxy formation (e.g., Blumenthal et al. 1986), and may even reveal properties of the dark matter particle such as cross sections for self-interactions (e.g., Spergel & Steinhardt 2000).

Nearby, galaxy centers can be studied directly with high spatial resolution observations. Hubble Space Telescope imaging of early-type galaxies shows that, contrary to theoretical expectations (e.g., Tremaine 1997), the luminosity profiles diverge at small radii (e.g., Faber et al. 1997; Ravindranath et al. 2001; Rest et al. 2001). The profiles seem to fall into two classes: “core” galaxies have a distinct transition between a steep outer profile and a shallow inner core that has  $I \propto R^{-\gamma}$  with  $\gamma \lesssim 0.3$ ; while “power law” galaxies show no such break and have steep central cusps with  $\gamma \gtrsim 0.5$ . Interestingly, the global properties of the galaxies seem to correlate well with the centers. Core galaxies tend to be luminous, slowly rotating systems with boxy or elliptical isophotes, while power law galaxies tend to be faint, rapidly rotating systems with disk isophotes. Although the division may not be as sharp as originally thought (see Ravindranath et al. 2001; Rest et al. 2001), it still puts strong constraints on the formation process. In hierarchical merging scenarios, simple models cannot easily explain why the large galaxies are so much less dense

than their small progenitors (see §7 of Faber et al. 1997, and references therein), and some additional process such as heating by binary black holes may be required (e.g., Milosavljevic & Merritt 2001; Milosavljevic et al. 2001).

For distant galaxies, we cannot directly resolve 10–100 parsec scales, but we can instead turn to a unique indirect probe offered by gravitational lensing. Lens theory predicts that if the central mass distribution is shallower than  $\rho \propto r^{-2}$  then any multiply-imaged gravitational lens must have an odd number of images (Burke 1981; Schneider, Ehlers & Falco 1992). Standard image configurations<sup>2</sup> have two or four bright images lying  $\sim 3$ –10 kpc from the center of the lens galaxy, with the remaining image just 10–100 pc from the center and much fainter than the others. Because the “core” image is very sensitive to the central surface density of the lens galaxy, with a higher density corresponding to a fainter image, it offers a unique way to constrain the density on scales that cannot be directly resolved. This probe of galaxy centers can in principle be applied to all lens galaxies, which now number more than 60 and are predominantly early-type galaxies spanning the redshift range  $z \sim 0.3$ –1 (e.g., Kochanek et al. 2000). It is conceptually equivalent to using radial arcs to constrain the central profiles of lensing clusters (e.g., Mellier, Fort & Kneib 1993; Smail et al. 1996; Molikawa & Hattori 2001; Oguri, Taruya & Suto 2001).

The best observational data on core images come from radio lenses, because the lack of radio emission from most lens galaxies enables sensitive searches for core images. The Cosmic Lens All-Sky Survey found 18 radio lenses but no core images, based on radio maps where the dy-

<sup>2</sup> The rare exception is a configuration where the source lies in a naked cusp (e.g., Schneider et al. 1992); among more than 60 known lenses, APM 08279+5255 is the only candidate naked cusp lens (Lewis et al. 2002). The only other exception is B1359+154, a unique lens where three lens galaxies jointly produce six bright images, and models predict three additional core images (Rusin et al. 2001).

<sup>1</sup> Hubble Fellow

dynamic range is typically several tens to several hundreds but reaches 1200 for B1030+074 and 2000 for B0218+357 (Rusin & Ma 2001; Norbury et al. 2002). Several other radio lenses have candidate core images (MG 1131+0456, Chen & Hewitt 1993; PMN J1632-0033, Winn et al. 2002) although the hypothesis that the central radio flux originates in the lens galaxy cannot be ruled out. At optical and near-infrared wavelengths, APM 08279+5255 has an odd number of images (Ibata et al. 1999; Egami et al. 2000), but its interpretation is not clear. The third image may be a core image, in which case it indicates a large low-density core in the lens galaxy (Ibata et al. 1999; Egami et al. 2000; Muñoz, Kochanek & Keeton 2001), or it may be a case of a “naked cusp” image configuration, in which case it contains no information about the center of the lens galaxy (Lewis et al. 2002). No other optical core images have been seen, although the searches are of course hindered by light from the lens galaxies.

The apparent discrepancy between data and theory provides the desired opportunity to learn about the centers of distant galaxies. Motivated both by theoretical expectations (see Tremaine 1997) and by ease of use, many analyses have assumed models with a finite density core and obtained limits on lens galaxy core radii (e.g., Narayan, Blandford & Nataraj 1984; Narasimha, Subramanian & Chitre 1986; Blandford & Kochanek 1987; Hinshaw & Krauss 1987; Narayan & Schneider 1990; Wallington & Narayan 1993; Kochanek 1996; Evans & Hunter 2002). Rusin & Ma (2001) instead used power law models and obtained a lower limit on the power law index,  $\gamma > 0.8$  at 90% confidence for a surface density  $\Sigma \propto R^{-\gamma}$ . The question remained, though, whether these two classes of models were realistic enough to provide robust, model independent conclusions about lens galaxy centers. Muñoz et al. (2001) introduced double power law models where the core region is allowed to have a power law cusp whose index is independent of the density profile at large radii. They found that the lack of a core image in B1933+503 robustly implies  $\gamma \gtrsim 0.6$  for that one galaxy. Keeton (2001) studied core images statistically using models with cuspy stellar components, treated as generalized Hernquist (1990) models, embedded in dark matter halos. He found that the models were inconsistent with the data, perhaps because generalized Hernquist models may not accurately represent the stellar components of galaxies on 10–100 pc scales.

The goal of this paper is to reconsider the core image problem using more realistic models derived from nearby galaxies, and more generally to discuss using core images as tools for studying the centers of distant ( $z \sim 0.3$ –1) galaxies. Nearby early-type galaxies have surface brightnesses that can be modeled as a Nuker law (Lauer et al. 1996; Byun et al. 1996), and in §2 we discuss lensing by such galaxies. In §3 we consider in a general way what physical properties of lens galaxies determine core image properties, or conversely what we can learn about lens galaxies by studying core images. In §4 we study in detail the core images predicted by a sample of realistic lens galaxies. Finally, in §5 we offer a summary and conclusions. We assume the popular  $\Lambda$ CDM cosmology with matter density  $\Omega_M = 0.3$ , cosmological constant  $\Omega_\Lambda = 0.7$ , and Hubble constant  $H_0 = 75 \text{ km s}^{-1} \text{ Mpc}^{-1}$ .

## 2. NUKER LAW LENSES

The lensing properties of a galaxy with projected mass density  $\Sigma$  are given by the lensing potential  $\phi$  that satisfies the two-dimensional Poisson equation  $\nabla^2 \phi = 2\Sigma/\Sigma_{\text{cr}}$ . Here  $\Sigma_{\text{cr}} = (c^2 D_{\text{ol}})/(4\pi G D_{\text{ol}} D_{\text{os}})$  is the critical surface density for lensing, where  $D_{\text{ol}}$ ,  $D_{\text{os}}$ , and  $D_{\text{ls}}$  are angular diameter distances between the observer (“o”), the lens (“l”), and the source (“s”). We consider a fiducial lensing situation with a lens galaxy at redshift  $z_l = 0.5$  and a source at redshift  $z_s = 2$ , which yields a critical density of  $\Sigma_{\text{cr}} = 2230 M_\odot \text{ pc}^{-2}$  for our adopted  $\Lambda$ CDM cosmology. The lensing deflection is given by  $\alpha = \nabla\phi$ , and the magnification depends on the second derivatives of  $\phi$ . See the book by Schneider et al. (1992) for a full discussion of lens theory.

Because lensing selects galaxies by mass, the sample of observed lens galaxies is dominated by early-type galaxies. In many nearby early-type galaxies the surface brightness distribution is well described by a Nuker law (Lauer et al. 1995; Byun et al. 1996),

$$I(R) = 2^{(\beta-\gamma)/\alpha} I_b \left(\frac{R}{r_b}\right)^{-\gamma} \left[1 + \left(\frac{R}{r_b}\right)^\alpha\right]^{(\gamma-\beta)/\alpha}, \quad (1)$$

where  $\gamma$  and  $\beta$  are the inner and outer power law indices, respectively,  $r_b$  is the radius where the break in the power law occurs,  $\alpha$  gives the sharpness of the break, and  $I_b$  is the surface brightness at the break radius. If the luminosity distribution has circular symmetry and the mass-to-light ratio is  $\Upsilon$ , the lensing deflection is

$$\alpha_{\text{gal}}(R) = \frac{2^{1+(\beta-\gamma)/\alpha}}{2-\gamma} \kappa_b r_b \left(\frac{R}{r_b}\right)^{1-\gamma} \times {}_2F_1 \left[ \frac{2-\gamma}{\alpha}, \frac{\beta-\gamma}{\alpha}, 1 + \frac{2-\gamma}{\alpha}, -\left(\frac{R}{r_b}\right)^\alpha \right], \quad (2)$$

where  $\kappa_b = \Upsilon I_b/\Sigma_{\text{cr}}$  is the surface mass density at the break radius in units of the critical density for lensing, and  ${}_2F_1$  is the hypergeometric function. If the stellar distribution has ellipsoidal symmetry, the lensing deflection must be computed numerically using the formalism given by, e.g., Schramm (1990).

Most galaxies contain central, supermassive black holes (e.g., Magorrian et al. 1998), so we consider adding them to the model. The deflection from a black hole is  $\alpha_{\text{bh}}(R) = R_E^2/R$  where the black hole’s Einstein radius is (in angular units)

$$R_E = \left[ \frac{4GM_\bullet}{c^2} \frac{D_{\text{ls}}}{D_{\text{ol}}D_{\text{os}}} \right]^{1/2}. \quad (3)$$

We normalize the black holes using the observed correlation between the black hole mass  $M_\bullet$  and the velocity dispersion  $\sigma$  of the parent galaxy (Gebhardt et al. 2000; Merritt & Ferrarese 2001). The net deflection is simply the sum of the deflections from the Nuker component and the black hole.

As an example we consider the nearby galaxy NGC4486, which has Nuker parameters  $\alpha = 2.82$ ,  $\beta = 1.39$ , and  $\gamma = 0.25$  and is a fairly typical (albeit massive) example of the early-type galaxies in the sample studied by Faber et al. (1997). We imagine a lens galaxy obtained by moving NGC4486 to a typical lens redshift  $z_l = 0.5$ . The deflection profile  $\alpha(R)$  for the resulting lens is shown

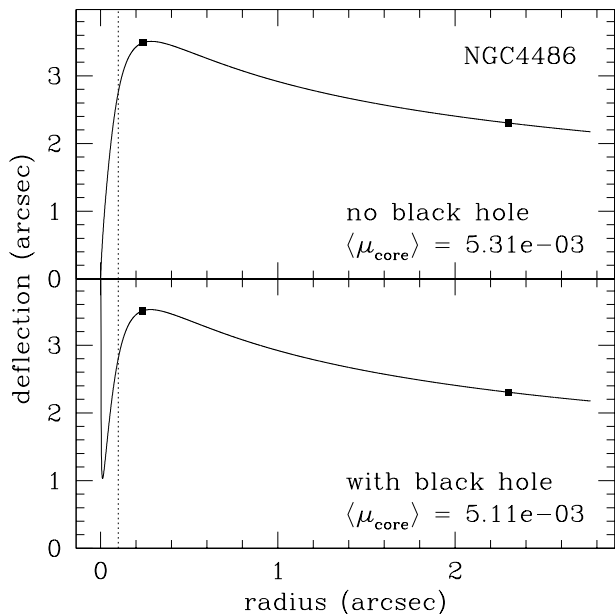


FIG. 1.— The deflection profile for a mock lens galaxy obtained by taking the nearby galaxy NGC4486 and moving it to redshift  $z_l = 0.5$ . The vertical dotted line indicates the Nuker break radius  $r_b$ . The dots mark the critical radii  $R_{\text{ein}}$  and  $R_{\text{rad}}$ . The top panel shows the result for the Nuker galaxy alone, while the bottom panel adds a central black hole normalized by the  $M_\bullet$ - $\sigma$  relation from Gebhardt et al. (2000). The mean core image magnification  $\langle \mu_{\text{core}} \rangle$  is computed with the method presented in §3.

in Fig. 1. The asymptotic behavior is  $\alpha(R) \propto R^{1-\gamma}$  for  $R \ll r_b$  (if there is no black hole), and  $\alpha(R) \propto R^{1-\beta}$  for  $R \gg r_b$ . Typical galaxies have  $\gamma < 1$  and  $\beta > 1$ , so the deflection is zero at the origin, rises to some finite peak, then slowly declines. There are two important radii corresponding to the “critical curves,” or curves along which the lensing magnification is infinite. The tangential critical curve lies at the Einstein radius  $R_{\text{ein}}$ , which is the solution to  $\alpha(R_{\text{ein}}) = R_{\text{ein}}$ . The radial critical curve lies at the radius  $R_{\text{rad}}$  which is the solution to  $d\alpha/dR = 1$ . The radial critical curve maps to a caustic at

$$u_{\text{max}} = \alpha(R_{\text{rad}}) - R_{\text{rad}}. \quad (4)$$

This caustic bounds the multiply-imaged region; sources with  $u < u_{\text{max}}$  are multiply-imaged, while sources with  $u > u_{\text{max}}$  are not. The core images are always contained in the region bounded by the radial critical curve. The radii  $R_{\text{ein}}$  and  $R_{\text{rad}}$  are marked in Fig. 1.

If the galaxy has a steep central cusp with  $\gamma > 1$ , the deflection diverges at the origin and is a monotonically decreasing function of radius. In this case, the radial critical curve does not exist and the lens never produces a core image. If the galaxy contains a central black hole, the black hole causes the deflection to diverge at the origin and suppresses some of the core images (Mao, Witt & Koopmans 2001). However, the black hole changes the deflection only at very small radii, so it has little effect on the critical radii  $R_{\text{ein}}$  and  $R_{\text{rad}}$  or on the mean core image magnification  $\langle \mu_{\text{core}} \rangle$  (see Fig. 1). Adding a dark matter halo to the lens galaxy would raise the outer deflection profile and make it approximately flat, but it would have little effect on the central deflection profile that determines the properties of the core images unless it were much more

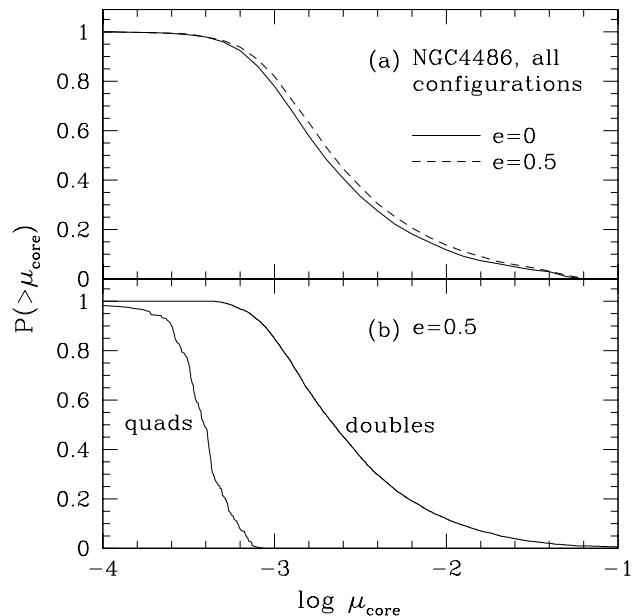


FIG. 2.— Cumulative distributions of magnification factors for the core images predicted by the NGC4486 mock lens galaxy. (a) Total distributions plotted for a circular (solid line) or flattened (dashed line) lens galaxy. (b) Distributions plotted separately for lenses with two or four bright images (doubles or quads), for a lens galaxy with ellipticity  $e = 0.5$ . There is more statistical uncertainty in the curve for quads than for doubles, because of the 7917 random source positions we examined only 238 of them corresponded to quads.

centrally concentrated than the light.

To characterize the core images expected in this lens, we study the core image magnification distribution. The distribution can be computed fairly rapidly using inverse ray shooting (e.g., Kayser, Refsdal & Stabell 1986; Wambsganss 1997). Fig. 2a shows the distribution for circular and flattened lens galaxies. The distribution is broad, spanning more than two orders of magnitude, with a median value  $\mu_{\text{core}} = 0.0019$  and a mean value  $\langle \mu_{\text{core}} \rangle = 0.0053$  for the circular case. Making the galaxy flattened shifts the magnification distribution to higher values; but even for ellipticity  $e = 0.5$  the shift is only 0.05 dex, so the core image magnification distribution is largely insensitive to ellipticity in the lens galaxy. (We would see more of an effect if we described core images by their flux ratio relative to the bright images,  $\mu_{\text{core}}/\mu_{\text{bright}}$ , because  $\mu_{\text{bright}}$  is quite sensitive to ellipticity.)

Ellipticity is important in one respect. If the lens galaxy is non-spherical, some source positions correspond to lenses with two bright images (doubles), while others correspond to lenses with four bright images (quads). (See, e.g., Schneider et al. 1992.) Fig. 2b shows the core image magnification distributions for quads and doubles separately. Because the source lie closer to the origin for quads than for doubles, and the core image magnification increases with the distance of the source from the origin, quads tend to have smaller core image magnifications than doubles. The quantitative details depend on the ellipticity, on any external tidal perturbation (shear) that may affect the lens, and on the stellar profile of the galaxy, but the general result is robust: quads tend to have smaller  $\mu_{\text{core}}$  than doubles.

The ellipticity effect combines with an observational se-

lection effect. Quads generally have larger total magnifications than doubles, so the sources in quads tend to be intrinsically fainter than the sources in doubles. Together, their fainter sources and smaller core image magnifications suggest that quads will tend to have fainter core images than doubles. The lack of core images in observed quads should therefore be less surprising than in doubles. Conversely, doubles should be better systems than quads for searching for core images.

Thus, while ellipticity in the lens galaxy is important in understanding differences between quads and doubles, it is not very important in the overall distribution of core image magnifications. In the remainder of the paper we therefore neglect ellipticity and use circular lens galaxies.

### 3. WHAT DO CORE IMAGES PROBE?

In order to derive meaningful conclusions from observational constraints on core images, it is important to understand how core images depend on the physical properties of lens galaxies. (Merely understanding the parameter dependencies in parametric lens models does not allow strong physical conclusions.) Although the full distributions of core images predicted for a particular lens galaxy must be computed numerically, the mean magnification  $\langle \mu_{\text{core}} \rangle$  can be studied analytically. Moreover, in §4 we argue that this quantity is actually a good way to characterize the distribution. Hence, in this section we study  $\langle \mu_{\text{core}} \rangle$  in general terms.

Formally, we have

$$\langle \mu_{\text{core}} \rangle = \frac{\int_{\text{mult}} \mu_{\text{core}}(\mathbf{u}) d\mathbf{u}}{\int_{\text{mult}} d\mathbf{u}}, \quad (5)$$

$$= \frac{\int_{\text{core}} d\mathbf{x}}{\int_{\text{mult}} d\mathbf{u}}. \quad (6)$$

The first line is simply the definition of the average, where the integral extends over the multiply-imaged region of the source plane. In the second line, the integral in the numerator extends over the “core” region in the image plane, defined to be the region within the radial critical curve; this equality holds because  $\mu_{\text{core}} = |\partial\mathbf{x}/\partial\mathbf{u}|$  is the Jacobian of the transformation between the source and image planes. In words, eq. (6) says that the mean core image magnification is equal to the area within the radial critical curve divided by the lensing cross section (the area of the multiply-imaged region in the source plane). For circularly symmetric lenses,

$$\langle \mu_{\text{core}} \rangle = (R_{\text{rad}}/u_{\text{max}})^2. \quad (7)$$

For non-circular lenses, Fig. 2 suggests that this is still a good approximation, because the  $\mu_{\text{core}}$  distribution is not terribly sensitive to ellipticity. These relations were first given by Keeton (2001).

Now we focus on circularly symmetric lenses. Given the definition of  $u_{\text{max}}$  from eq. (4), we can write eq. (7) as

$$\langle \mu_{\text{core}} \rangle = [\alpha(R_{\text{rad}})/R_{\text{rad}} - 1]^{-2}, \quad (8)$$

$$= (\langle \kappa \rangle_{R_{\text{rad}}} - 1)^{-2}, \quad (9)$$

where  $\langle \kappa \rangle_R$  is the mean surface density within radius  $R$ , in units of the critical density for lensing. The second equality holds because by the definition of the deflection,

$$\frac{\alpha(R)}{R} = \frac{2}{R^2} \int_0^R \xi \kappa(\xi) d\xi = \langle \kappa \rangle_R. \quad (10)$$

Alternatively, returning to eq. (8) and using the identities

$$\frac{\alpha(R)}{R} + \frac{d\alpha}{dR} = 2\kappa(R), \quad (11)$$

$$\left. \frac{d\alpha}{dR} \right|_{R_{\text{rad}}} = 1, \quad (12)$$

we obtain

$$\langle \mu_{\text{core}} \rangle = \frac{1}{4} [\kappa(R_{\text{rad}}) - 1]^{-2}. \quad (13)$$

Eqs. (9) and (13) indicate that the mean core image magnification is given very simply from either the surface mass density at the radial critical curve  $R_{\text{rad}}$  or the mean surface mass density within  $R_{\text{rad}}$ .

What remains is to understand what physical properties of the galaxy determine the radial critical curve  $R_{\text{rad}}$ . Equating eqs. (9) and (13), we find that  $R_{\text{rad}}$  is the solution to

$$2\kappa(R_{\text{rad}}) = \langle \kappa \rangle_{R_{\text{rad}}} + 1. \quad (14)$$

This relation implies that the radial critical curve is related to the concentration of galaxy’s (projected) mass distribution. We expect  $\kappa(R)$  to be a decreasing function, so  $\langle \kappa \rangle_R \geq \kappa(R)$  for all  $R$ . If  $\kappa(R)$  is steep (the mass is concentrated), then  $\langle \kappa \rangle$  is large and we must go to large  $\kappa$  (small  $R$ ) to satisfy eq. (14); eq. (13) then implies faint core images.<sup>3</sup> Conversely, if  $\kappa(R)$  is shallow then eq. (14) is satisfied at smaller  $\kappa$  (larger  $R$ ), and the core images are brighter.

These results can be demonstrated with two simple examples. First, consider a softened isothermal sphere with surface mass density  $\kappa(R) = (b/2)(s^2 + R^2)^{-1/2}$ , where  $s$  is a core radius and  $b$  is a scale radius that equals the Einstein radius in the case  $s = 0$ . The critical radii and mean core image magnification are

$$R_{\text{ein}} = [b(b - 2s)]^{1/2}, \quad (15)$$

$$R_{\text{rad}} = \frac{1}{2} \zeta(\xi + \zeta)^{1/2}(\xi - 3\zeta)^{1/2}, \quad (16)$$

$$u_{\text{max}} = \frac{1}{4} (\xi + \zeta)^{1/2}(\xi - 3\zeta)^{3/2}, \quad (17)$$

$$\langle \mu_{\text{core}} \rangle = \left( \frac{2\zeta}{\xi - 3\zeta} \right)^2, \quad (18)$$

where  $\xi = (4b + s)^{1/2}$  and  $\zeta = s^{1/2}$ . Decreasing the core radius reduces  $\langle \mu_{\text{core}} \rangle$ , with  $\langle \mu_{\text{core}} \rangle \approx s/b$  for  $s \ll b$ . Second, consider a power law density  $\rho \propto r^{-\gamma}$  or  $\kappa \propto R^{1-\gamma}$ , with  $\gamma > 1$  to ensure that  $\kappa(R)$  is a decreasing function. The critical radii and mean core image magnification are

$$R_{\text{rad}} = R_{\text{ein}} (2 - \gamma)^{1/(\gamma-1)}, \quad (19)$$

$$u_{\text{max}} = R_{\text{ein}} (\gamma - 1)(2 - \gamma)^{(2-\gamma)/(\gamma-1)}, \quad (20)$$

$$\langle \mu_{\text{core}} \rangle = \left( \frac{2 - \gamma}{\gamma - 1} \right)^2. \quad (21)$$

Increasing  $\gamma$  (making the profile steeper) decreases  $\langle \mu_{\text{core}} \rangle$ . These expressions are valid only for  $1 < \gamma < 2$ , because for  $\gamma > 2$  the density profile is so steep that the radial

<sup>3</sup> This result also explains how adding a central black hole affects the mean core image magnification. The black hole suppresses some core images, reducing  $\langle \mu_{\text{core}} \rangle$  (Mao et al. 2001). In the language of our analysis, the black hole increases  $\langle \kappa \rangle_R$  without changing  $\kappa(R)$ , so we must move to larger  $\kappa$  (smaller  $R$ ) to keep eq. (14) satisfied.

critical curve does not exist and the model does not produce core images. Previous studies used models like these to understand the inverse relation between the brightness of core images and the concentration of the lens galaxy, but eqs. (13) and (14) now give it in a general, model independent form.

#### 4. CORE IMAGES IN REALISTIC GALAXIES

##### 4.1. The sample

To understand core images in realistic galaxies, we study models constructed from a sample of observed galaxies. This approach ensures that we examine the region of parameter space occupied by real systems. We seek galaxies with well resolved luminosity profiles, plus measured velocity dispersions as mass indicators. Faber et al. (1997), Carollo et al. (1997), Carollo & Stiavelli (1998), and Ravindranath (2001) have published samples of nearby early-type galaxies observed with high-resolution Hubble Space Telescope imaging at optical or near-infrared wavelengths.<sup>4</sup> Together the samples comprise 73 distinct galaxies with both Nuker law fits and velocity dispersions, which are summarized in Table 1. The different samples use different passbands: V for the Faber sample, H for the Ravindranath sample, and V and I for the Carollo sample. However, we can check for wavelength dependence and other systematic effects because some of the galaxies appear in more than one sample: six galaxies in both the Faber and Ravindranath samples, five galaxies in both the Faber and Carollo samples, six galaxies in both the Ravindranath and Carollo samples, and ten galaxies with multiple passbands in the Carollo sample. (No galaxies appear in all three samples.)

We use this sample to construct mock lens galaxies by moving each galaxy to a typical lens redshift  $z_l = 0.5$ , and assuming a typical source redshift  $z_s = 2$ . Following Faber et al. (1997), we compute the mass-to-light ratio for each galaxy using a spherical and isotropic dynamical model. Faber et al. (1997) give mass-to-light ratios for their sample, providing a check for our calculations. We then compute the lensing properties of the mock lens galaxies, which are summarized in Table 1.

As discussed in §2 we focus on circularly symmetric galaxies because ellipticity has little effect on the overall distribution of core image magnifications. We consider only the Nuker components of the galaxies, neglecting any nuclear components that may be indicated by fits to the surface brightness distribution. This is a conservative approach to our problem, because any additional mass concentration would decrease the predicted core image magnifications and bring the models closer to agreement with the data. We also neglect dark matter halos. Dark matter does not appear to be dynamically important in the inner 5–10 kpc of elliptical galaxies (e.g., Gerhard et al. 2001). While it is important for lensing (because lensing depends on the projected mass; e.g., Treu & Koopmans 2002), dark matter would have little effect on the projected mass distributions on the  $\lesssim 200$  pc scales important for core images unless it were substantially more concentrated than the light.

We can check that our mock lenses are reasonable in sev-

<sup>4</sup> Rest et al. (2001) give a similar sample, but without velocity dispersions.

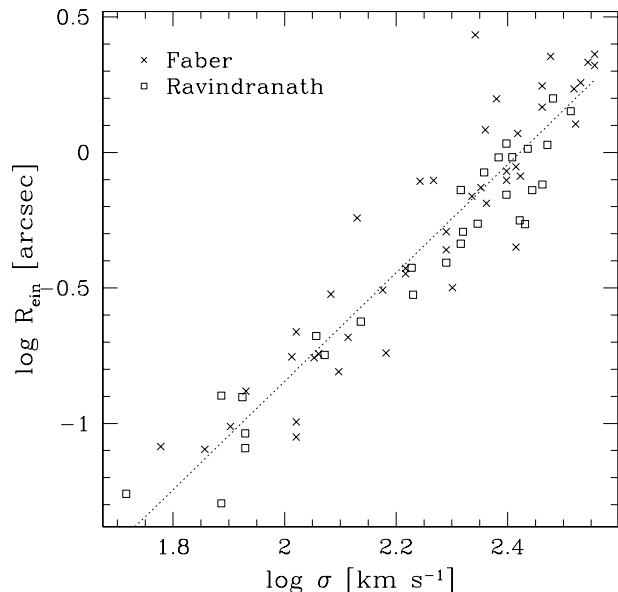


FIG. 3.— Relation between the velocity dispersion  $\sigma$  and Einstein radius  $R_{\text{ein}}$  for the mock lens galaxies. Crosses and boxes indicate galaxies in the Faber and Ravindranath samples, respectively. The dotted line shows the relation  $R_{\text{ein}} \propto \sigma^2$ ; the fitted zero point is  $-4.84$  (in log units), compared with a predicted value of  $-4.74$  for comparable Singular Isothermal Spheres.

eral ways. First, we compute the Einstein radius for each galaxy and compare it to the velocity dispersion in Fig. 3; this tests whether the lensing and dynamical masses are consistent. For comparison, a simple Singular Isothermal Sphere (SIS) lens has the scaling  $R_{\text{ein}} \propto \sigma^2$ , with a zero point of  $-4.74$  (in log units) for  $z_l = 0.5$  and  $z_s = 2$  in our adopted  $\Lambda$ CDM cosmology (see Schneider et al. 1992). The mock galaxies are consistent with this scaling and a fitted zero point of  $-4.84$ , although with a scatter of 0.16 dex. The fact that the mock galaxies lie on average 0.1 dex below the expected SIS relation may be related to our neglect of dark matter halos. Still, the dynamical and lensing properties are related in a sensible way suggesting that the mock lens galaxies are not unreasonable.

As a second check, we consider the galaxies that appear in more than one of the original samples. For example, for each galaxy that was observed and modeled by both Faber et al. (1997) and Ravindranath et al. (2001), we compute the lensing properties using both models and compare them. In this way we test whether the use of different modeling techniques and different passbands affects our lensing results. Fig. 4 compares the Einstein radii and mean core image magnifications for all of the duplicate galaxies. There is fair agreement in the Einstein radii, although with some scatter because different studies find somewhat different values of the outer slope  $\beta$ ; the main outlier is NGC524, where dust is known to affect the luminosity profile at optical wavelengths (Lauer et al. 1995; Ravindranath et al. 2001). There is good agreement in the mean core image magnification, so our conclusions about the properties of core images are not sensitive to whose data we use. For the remainder of the paper, we adopt as our main sample all of the Ravindranath galaxies plus the Faber galaxies that are not in the Ravindranath sample.

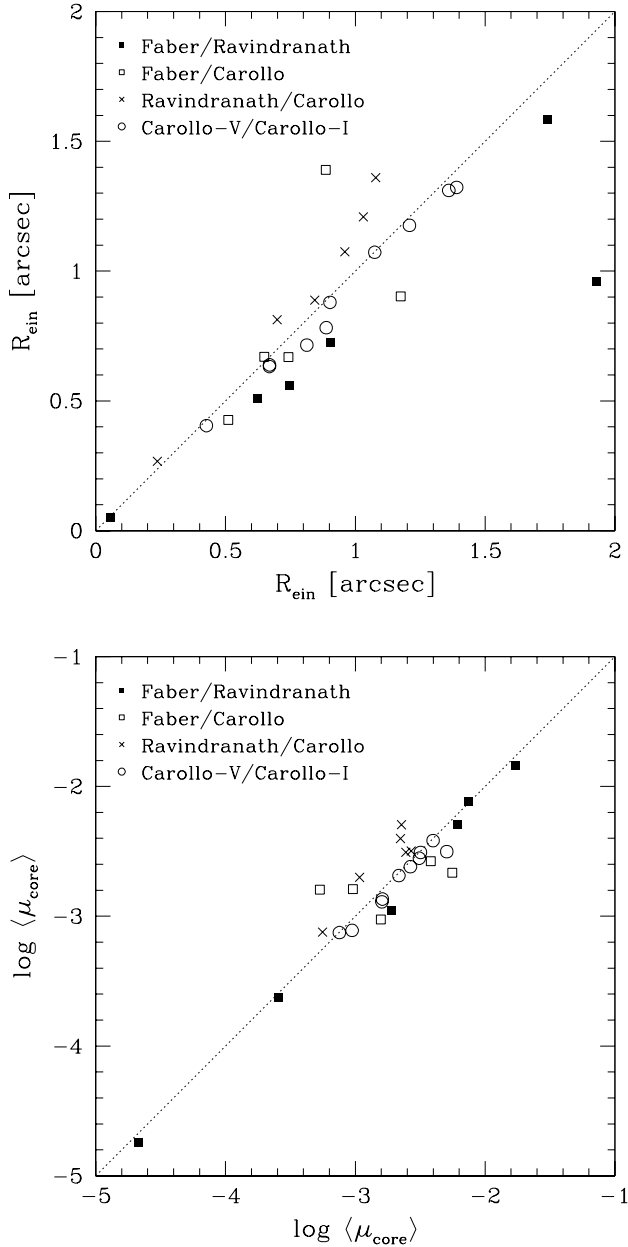


FIG. 4.— A comparison of the Einstein radii (top) and mean core image magnifications (bottom) for galaxies that appear in more than one of the original samples. Filled boxes indicate galaxies in both the Faber and Ravindranath samples, open boxes the Faber and Carollo samples, and crosses the Ravindranath and Carollo samples. Open circles indicate galaxies in both the V-band and I-band Carollo samples.

#### 4.2. A plethora of core images

Fig. 5a shows the core image magnification distributions for nine of the mock lens galaxies to illustrate the range of effects. Each mock lens galaxy has a distribution of core image magnifications that spans some two orders of magnitude, and the complete set of mock lenses spans six orders of magnitude in  $\mu_{\text{core}}$ . Realistic lens galaxies predict a remarkably wide range of core images.

Studying the full  $\mu_{\text{core}}$  distribution for each mock lens galaxy is impractical, so we would like to describe each

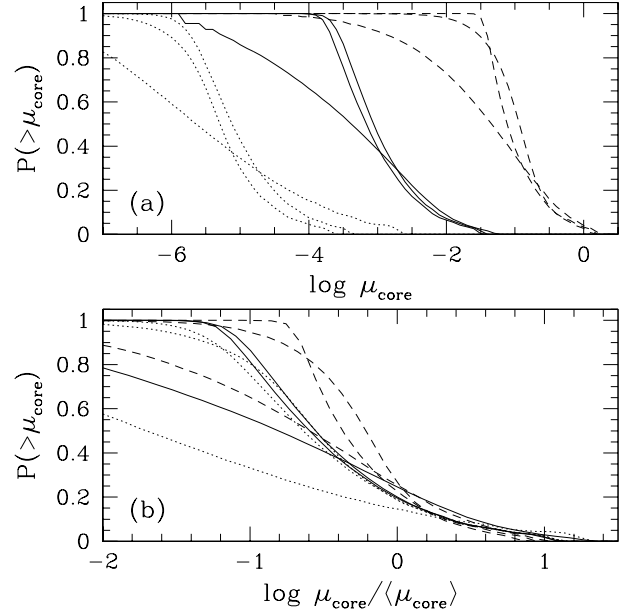


FIG. 5.— Cumulative core image magnification distributions for nine of the mock lens galaxies: the three with the lowest non-zero values for  $\langle \mu_{\text{core}} \rangle$  (dotted lines; NGC221, NGC3377, NGC4621); the three with values for  $\langle \mu_{\text{core}} \rangle$  at the median of the sample (solid lines; NGC4570, NGC5982, NGC4649); and the three with the largest values for  $\langle \mu_{\text{core}} \rangle$  (dashed lines; NGC4239, NGC6166, NGC5273). (a) Distributions of the core image magnification  $\mu_{\text{core}}$ . (b) Distributions of the normalized magnification  $\mu_{\text{core}} / \langle \mu_{\text{core}} \rangle$ .

galaxy by a single characteristic quantity. We propose to use the mean core image magnification  $\langle \mu_{\text{core}} \rangle$  as a good characteristic value, partly because this quantity is easy to compute (see §3), and partly because Fig. 5b suggests that it is indeed characteristic of the overall distribution. Specifically, when plotted in terms of the normalized quantity  $\mu_{\text{core}} / \langle \mu_{\text{core}} \rangle$  the distributions for a wide range of galaxies all lie on top of each other. Although there are differences in the shapes of the distributions at the faint end, the distributions at the bright end are remarkably similar. Hence, we believe that  $\langle \mu_{\text{core}} \rangle$  is a useful characterization of the distribution of core image magnifications for a particular galaxy, especially at the bright end.

Fig. 6 shows a histogram of the  $\langle \mu_{\text{core}} \rangle$  values for the 73 mock lens galaxies. (The values are given in Table 1.) Note that the histogram is intended only to show the broad range of core image properties in our sample; it should not be interpreted as a global distribution of  $\langle \mu_{\text{core}} \rangle$  values, because our sample is not a statistical sample of galaxies. Still, the histogram is instructive in illustrating that the mean values  $\langle \mu_{\text{core}} \rangle$  span more than four orders of magnitude, from  $\langle \mu_{\text{core}} \rangle = 1.8 \times 10^{-5}$  for NGC221 to  $\langle \mu_{\text{core}} \rangle = 0.19$  for NGC5273 — plus two galaxies that never produce core images (NGC1172 and NGC4742). Again we see the wide range of core image properties in realistic lens galaxies; some lenses should have bright, detectable core images, while others should have core images that are essentially invisible.

In principle the central supermassive black holes that are common in galaxies can suppress core images (Mao et al. 2001), but in practice they have little effect. Table 1 gives the values for  $\langle \mu_{\text{core}} \rangle$  when the galaxies contain black holes

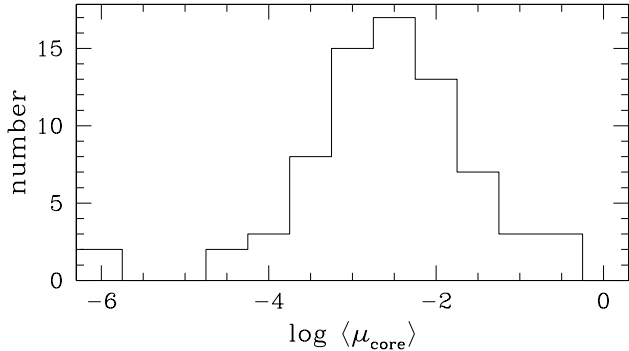


FIG. 6.— Histogram of the mean core image magnifications for the 73 mock lens galaxies. Galaxies that do not produce core images are arbitrarily placed at  $\log \langle \mu_{\text{core}} \rangle = -6$ .

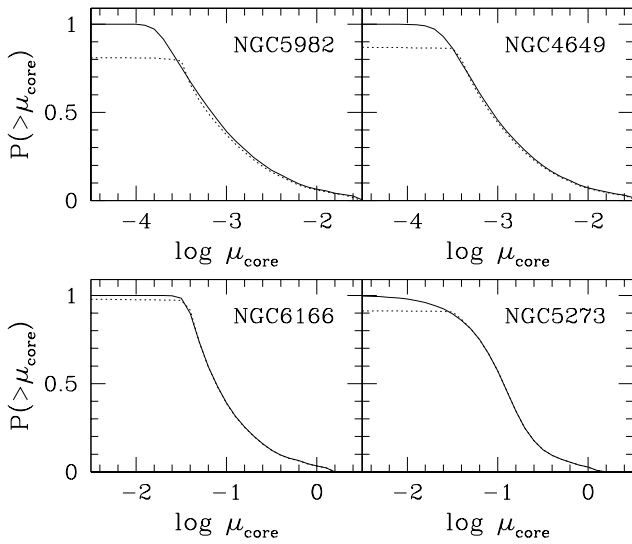


FIG. 7.— Core image magnification distributions for galaxies with (dotted lines) and without (solid lines) central supermassive black holes, for four of the galaxies from Fig. 5. Black holes can suppress core images (see Mao et al. 2001), but only at the faint end of the core image distribution.

normalized by the  $M_{\bullet}$ - $\sigma$  relations measured by Gebhardt et al. (2000) and Merritt & Ferrarese (2001). In a few cases the black hole modifies the central potential enough to erase all core images (NGC221, NGC3115, NGC3377, NGC3900, NGC4464, NGC4467, NGC4621, and NGC5838). But all of these cases have  $\langle \mu_{\text{core}} \rangle \leq 0.001$  even without a black hole, which suggests that adding a black hole can erase all core images only if the core images are faint to begin with. In the remaining cases the black hole reduces  $\langle \mu_{\text{core}} \rangle$  by only about 0.1 dex. The black hole does suppress some core images, but only at the *faint* end of the distribution, as shown in Fig. 7. In other words, black holes have little effect on the core images in realistic lens galaxies, especially at the bright end of the core image distribution. Black holes therefore fail to resolve the core image paradox. These conclusions are based on local measurements of the  $M_{\bullet}$ - $\sigma$  relation, which may not hold at higher redshifts; but black holes would have to be substantially more massive (relative to their parent galaxies) at  $z \sim 0.5$  than at  $z = 0$  in order to change our conclusions. Another possibility is that binary black holes are

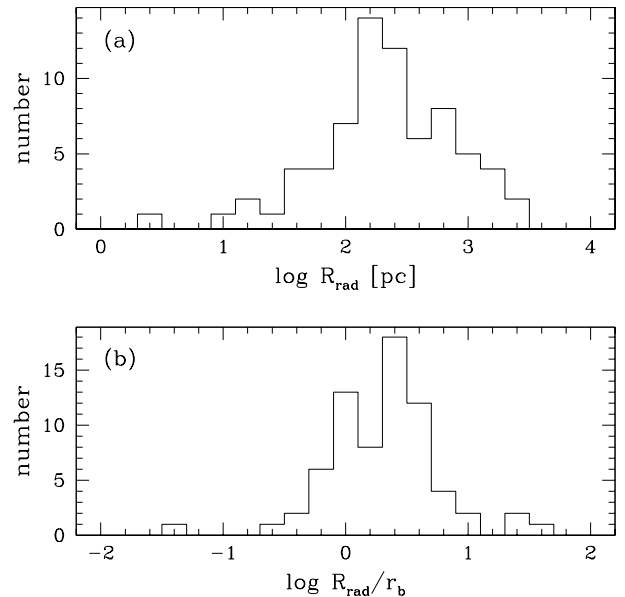


FIG. 8.— Histograms of the lensing critical radius  $R_{\text{rad}}$ , which bounds the core image region. (a) The critical radius in parsecs. (b) The ratio of the critical radius to the Nuker break radius  $r_b$ . Galaxies that lack a critical radius  $R_{\text{rad}}$  are not included.

common in galaxies at  $z \sim 0.5$ . In principle binary black holes can be more effective than single black holes at suppressing core images, but for realistic binary parameters the differences are small and binary black holes do not strongly suppress core images (Keeton & Zhao, in prep.). In the remainder of the paper we neglect black holes.

We now seek to understand the diversity of core image properties in the mock lens galaxies, and to identify the galaxy properties that affect the core images. First, we examine the region of the galaxy that is probed by core images. Recall that the core images are always contained within the inner lensing critical curve, which has radius  $R_{\text{rad}}$  (see §2). Fig. 8 shows that the core image region has a characteristic scale  $\sim 200$  pc (the median value of  $R_{\text{rad}}$  for the sample), and is comparable to or slightly larger than the Nuker break radius. Thus, core images probe the inner tens to hundreds of parsecs at the centers of galaxies.

Next, we consider how the mean core image magnification  $\langle \mu_{\text{core}} \rangle$  depends on various properties of the galaxies, as shown in Fig. 9. The interesting general result is that no single property of a galaxy strongly determines its core image properties. There is no simple relation between  $\langle \mu_{\text{core}} \rangle$  and the outer and inner Nuker power law indices  $\beta$  and  $\gamma$  (Figs. 9a and 9b). This result makes sense in combination with Fig. 8: the lensing critical radius  $R_{\text{rad}}$  is often comparable to the Nuker break radius  $r_b$ , so we are in a regime where the galaxy cannot be described as a simple power law, and  $\langle \mu_{\text{core}} \rangle$  is not dominated by either  $\beta$  or  $\gamma$  separately. The distinction between “core” and “power law” galaxies seen in their luminosity profiles and dynamics (Faber et al. 1997) does not appear to carry over into lensing and core images. There is likewise no simple relation between  $\langle \mu_{\text{core}} \rangle$  and galaxy mass (as represented by velocity dispersion; Fig. 9c); galaxies with a given  $\sigma$  have  $\langle \mu_{\text{core}} \rangle$  values that range over some three orders of magni-

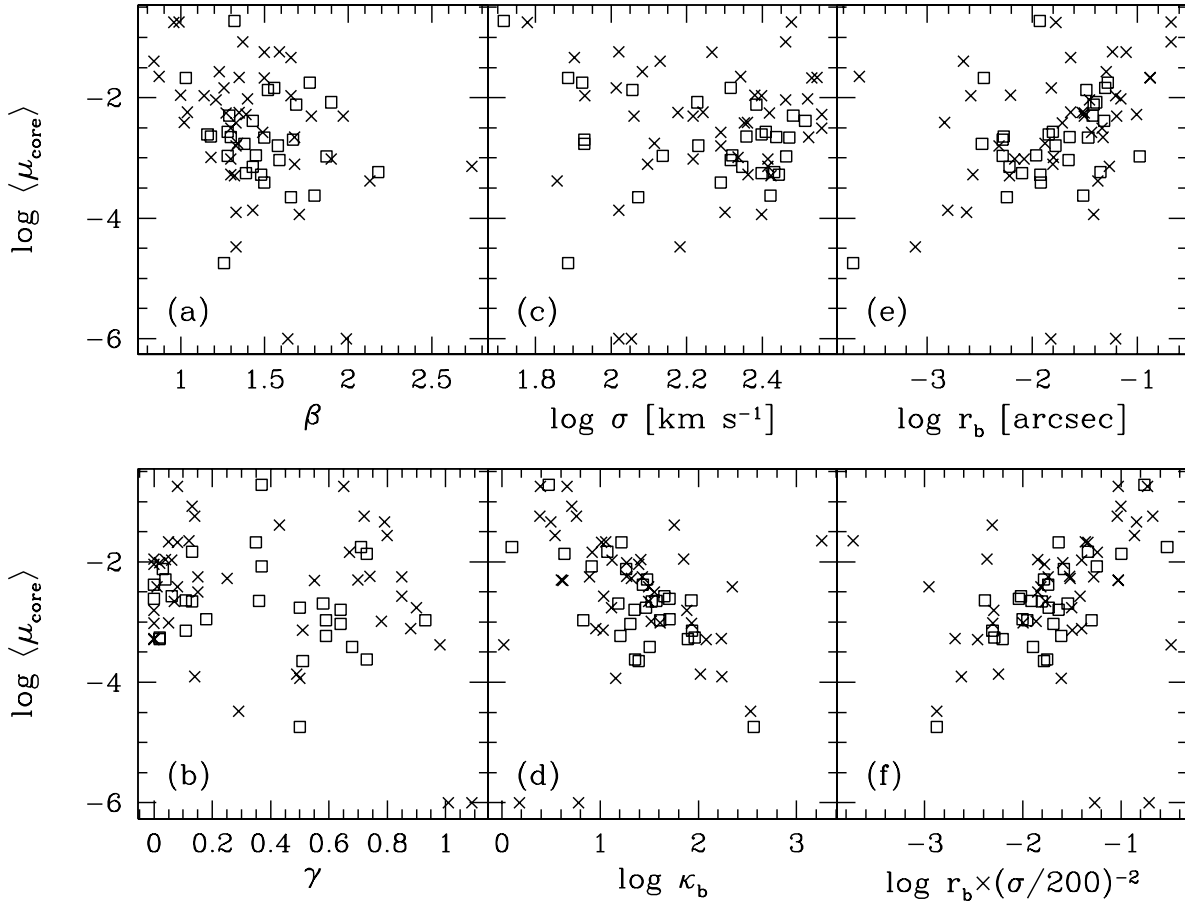


FIG. 9.— Scatter plots of the mean core image magnifications  $\langle \mu_{\text{core}} \rangle$  versus various galaxy properties. Crosses and boxes indicate galaxies in the Faber and Ravindranath samples, respectively. Galaxies that do not produce core images are arbitrarily placed at  $\log(\mu_{\text{core}}) = -6$ .

tude or more. Dwarf galaxies are not systematically more or less likely than giant galaxies to produce bright core images.

Based on the arguments in §3 we expect a connection between the core image properties and some measure of the concentration of the mass distribution. There is a trend between  $\langle \mu_{\text{core}} \rangle$  and the surface density at the break radius ( $\kappa_b$ , Fig. 9d): galaxies with higher break densities tend to predict fainter core images. There is also a general trend between with the Nuker break radius  $r_b$  (Fig. 9d): galaxies with smaller break radii, and hence smaller core regions, tend to predict fainter core images. But this trend is neither strong nor tight, because by itself  $r_b$  cannot distinguish between galaxies that are large and highly concentrated and those that are less concentrated but intrinsically small. One way to remove this effect is to normalize the break radius using the Einstein radius as a measure of the global scale of the galaxy; because  $R_{\text{ein}} \propto \sigma^2$ , we actually use  $r_b/\sigma^2$  (Fig. 9f). These three trends all indicate that there is indeed some connection between the core images and the concentration of the galaxy such that more concentrated galaxies tend to predict fainter core images. However, the trends have significant scatter and thus are not highly predictive. In other words, there does not appear to be a simple measure of a galaxy’s concentration that strongly determines its core image properties.

To summarize, realistic lens galaxies have an extremely wide range of core image properties; some should have bright, detectable core images, while others should have core images that are very faint or absent altogether. A galaxy’s core image properties are related to its mass concentration, but there does not appear to be any simple measure of concentration that yields a clean prediction of the core image properties. The complication is that in Nuker law lenses the lensing critical radius  $R_{\text{rad}}$  tends to be comparable to the break radius  $r_b$ , which means that all of the Nuker parameters affect the core image properties. This conclusion has a somewhat surprising corollary. We might expect that the distinction between “core” and “power law” galaxies, with their different luminosity profiles, would be obvious in their core image properties, but it is not.

#### 4.3. Should we see core images?

We can now re-evaluate the core image problem in terms of our expectations for realistic lens galaxies. Although our sample is not a proper statistical sample of galaxies, if we assume that it does at least represent the range of realistic galaxy properties then we can consider whether the lack of observed core images is surprising or not. The main issue is to understand what types of lens galaxies produce bright core images and whether we should expect to find



many lenses from such galaxies. There are three galaxies in the sample with  $\langle \mu_{\text{core}} \rangle > 0.1$ : two are dwarf galaxies (NGC4239 and NGC5273), while the third is a giant elliptical at the center of a cluster (NGC6166). Because lensing selects galaxies by mass it tends to select against dwarf galaxies, so even if some dwarf galaxies are good at producing core images they are unlikely to produce lenses in the first place. As for NGC6166, it is unusual for being a brightest cluster galaxy as well as the most distant (120 Mpc) and least concentrated (lowest surface brightness and largest break radius) galaxy in the Faber et al. (1997) sample. Thus, it appears to be an atypical galaxy drawn from the tail of the galaxy population. Statistically, lensing is not likely to select rare galaxies to be lens galaxies.

Lensing selection effects are important for core images in another way. Consider a set of galaxies that are similar to each other, specifically a set of galaxies with the same Einstein radius. Within this set, are galaxies that predict bright core images any more or less likely to be selected for lensing than galaxies that predict faint core images? Fig. 10 shows the lensing cross section, normalized by the area within the Einstein ring, versus  $\langle \mu_{\text{core}} \rangle$ . There is a clear decrease in the normalized cross section with increasing  $\langle \mu_{\text{core}} \rangle$ , and it does not depend on whether magnification bias is included or omitted. The trend for the mock lens galaxies agrees well with analytic predictions for simple softened power law lens models. At fixed Einstein radius, then, galaxies that predict bright core images have smaller lensing cross sections than galaxies that predict faint core images, so they are less likely to be selected for lensing. There is an intrinsic bias against lenses with bright core images.

Thus, the types of galaxies that can produce bright core images are probably not common, and they have small lensing cross sections relative to galaxies that are comparably massive but produce faint core images. The two effects combine to suggest that bright core images are not likely to be prevalent in observed lens samples.

#### 4.4. Comparison with data

The observational constraints on core images take the form of upper limits on the core image flux  $f_{\text{core}}$  in observed lenses. The magnification cannot be directly constrained because the intrinsic flux of the source is unknown. One way around this problem is to use the flux ratio of the core image to the brightest image, because the source flux factors out to leave  $f_{\text{core}}/f_{\text{bright}} = \mu_{\text{core}}/\mu_{\text{bright}}$ . This approach requires explicitly solving the lens equation to find all images, and thus is valuable for applications like lens modeling where the lens equation must be solved anyway (e.g., Muñoz et al. 2001). While it can be used for statistical analyses (e.g., Rusin & Ma 2001; Keeton 2001), it eliminates technical simplifications like the ability to compute  $\langle \mu_{\text{core}} \rangle$  rapidly without solving the lens equation (but see Evans & Hunter 2002 for a different kind of technical simplification). It also makes the conclusions sensitive to quantities like ellipticity in the lens galaxy, because  $\mu_{\text{core}}$  is fairly insensitive to ellipticity but  $\mu_{\text{bright}}$  is not.

An alternate approach is to fit a lens model to the observed images to constrain the source flux, and then combine the inferred source flux with the limits on  $f_{\text{core}}$  to

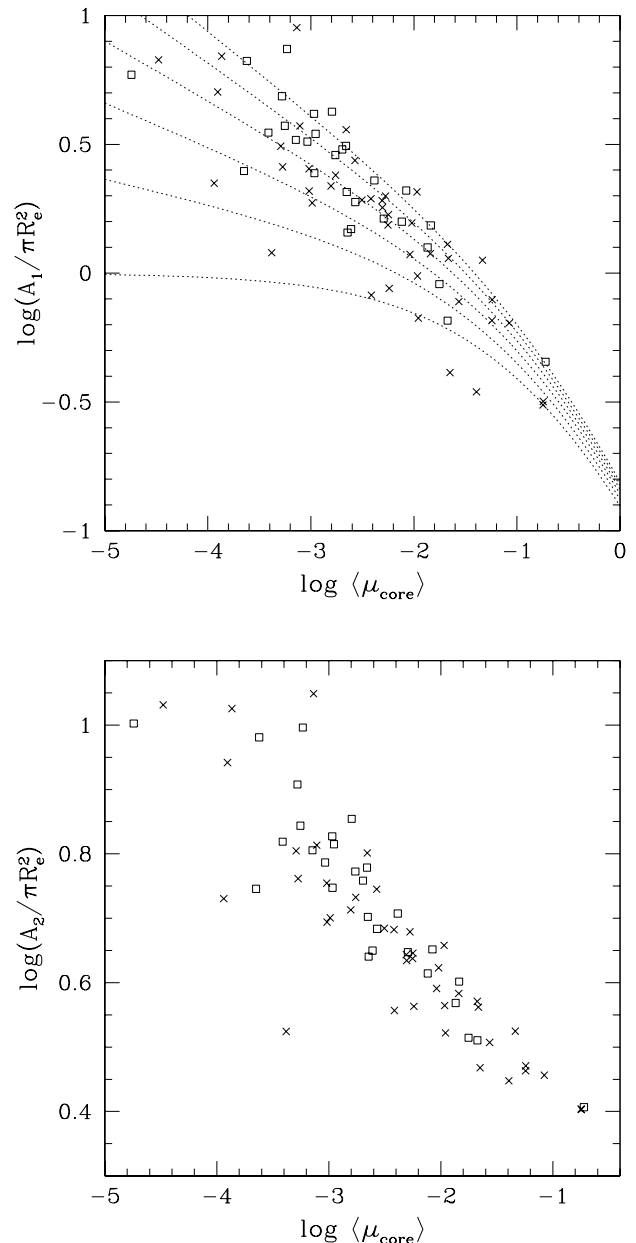


FIG. 10.— Scatter plots of the lensing cross section versus the core image magnification. The cross sections are normalized by the area within the Einstein ring,  $\pi R_{\text{ein}}^2$ . (Top)  $A_1$  is the simple lensing cross section, or the area of the multiply-imaged region in the source plane. The curves show results for simple softened power law lens models  $\Sigma \propto (s^2 + R^2)^{-\beta}$  with  $\beta = 1.0, 1.1, 1.2, 1.3, 1.4,$  and  $1.5$  from bottom to top. (Bottom)  $A_2$  is the lensing cross section corrected for magnification bias.

put limits on  $\mu_{\text{core}}$ . This approach should be robust because the model properties that determine the source flux from the observed images (the enclosed mass on 3–10 kpc scales) decouple from the properties that affect core images (the density profile on  $\lesssim 200$  pc scales). With this approach, Norbury et al. (2002) obtain upper limits on  $\mu_{\text{core}}$  for 15 radio lenses from the Cosmic Lens All-Sky Survey, as shown in Fig. 11.

For an accurate comparison we need a prediction of the overall  $\mu_{\text{core}}$  distribution from the models (not merely the

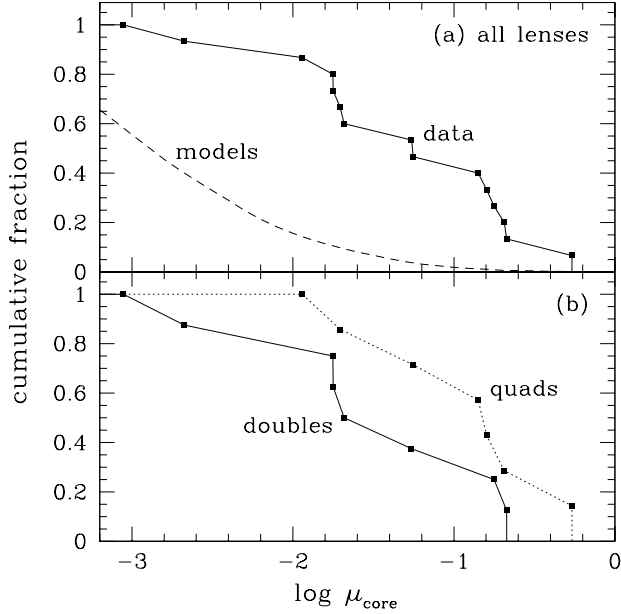


FIG. 11.— Upper limits on core image magnifications for 15 observed radio lenses (Norbury et al., in prep.). The points show  $5\sigma$  upper limits on  $\mu_{\text{core}}$ . (a) The data for all lenses. The dashed curve shows the net  $\mu_{\text{core}}$  distribution predicted by a weighted sum of the model galaxies (see text). (b) The data for doubles and quads shown separately.

set of  $\langle \mu_{\text{core}} \rangle$  values for the sample galaxies, as in Fig. 6). A proper prediction is impossible because, again, our sample is not a statistical sample of galaxies. Nevertheless, for the sake of comparison we naïvely combine our sample by summing all of the  $\mu_{\text{core}}$  distributions (a few of which are shown in Fig. 5), weighting each galaxy by its lensing cross section. The result is shown as the dashed curve in Fig. 11. It is interesting to see that the model predictions lie well below the limits from the data. The model does not predict that core images should be brighter than observed. In fact, it suggests that the observational sensitivity may need to improve by more than an order of magnitude before detections of core images become common. Despite concerns that the model sample is not statistically complete, we believe that the general conclusion is reliable. Galaxies that produce bright core images would have to be substantially more common in the universe than in our sample in order to make the model predictions inconsistent with the current observational data.

Evans & Hunter (2002) reach similar conclusions from an analysis of softened power law potential models. They argue that the break radii in the galaxies observed by Faber et al. (1997) are small enough to make core images faint even if the galaxies have simple finite-density cores. Although we believe our models to be more realistic because they allow more general cores and are constructed directly from the fitted profiles, it is reassuring that the conclusions are consistent.

We previously found that Hernquist model galaxies predict core images to be more common than observed (Keeton 2001). Like a Nuker law, a Hernquist model has a steep outer profile that smoothly changes to a shallow central cusp, but with a larger transition radius. Our new models should be more realistic because they are based on fits

to the luminosity profiles of observed galaxies, which have small transition radii. The smaller break radii mean higher central densities and thus fainter predicted core images.

Another interesting result from the data is that the upper limits from quads are weaker than the upper limits from doubles (Fig. 11b). The flux limits for the various lenses are comparable, but the quads tend to have fainter sources. Combining this result with our prediction that quads will tend to have fainter core images than doubles (Fig. 2b), we conclude that the lack of core images in observed quad lenses is no surprise at all.

## 5. CONCLUSIONS

Core images in strong gravitational lens systems provide a unique probe of the centers of galaxies at redshifts  $z \sim 0.2$ –1. The brightnesses of core images are determined by the density profiles of galaxies inside  $\lesssim 200$  pc. The lack of core images in observed lenses, especially in radio lenses, sets strong lower limits on the central densities of the lens galaxies (e.g., Wallington & Narayan 1993; Muñoz et al. 2001).

The mapping between core images and galaxy centers can be studied in two directions. In the forward problem knowledge of galaxy centers is used to make predictions about core images. Based on the first lens models drawn directly from the resolved stellar mass distributions of nearby early-type galaxies, we predict that real galaxies should produce a remarkably wide range of core images. Some should have bright core images (magnification  $\mu_{\text{core}} \gtrsim 0.1$ ), while many others will have core images that are faint ( $\mu_{\text{core}} \lesssim 0.001$ ) or absent altogether.

Qualitatively, more concentrated galaxies produce fainter core images. Quantitatively, however, there does not seem to be a simple predictive relation between observed galaxy properties and core images. Lensing is biased against galaxies with bright core images, because they have smaller cross sections than comparable galaxies with faint core images. Four-image lenses should tend to have fainter core images than two-image lenses, because in quads the source is always close to the center of the lens galaxy where the core image magnification is low. Supermassive black holes in the centers of galaxies can suppress faint core images, but they have little effect on bright core images or on the mean magnification.

The connection between core images and galaxy centers can also be studied in the inverse problem, where the analysis of core image data yields constraints on the centers of lens galaxies. Previous work placed limits on the core radius or on the logarithmic slope of the density (e.g., Wallington & Narayan 1993; Rusin & Ma 2001), but it was not clear how model dependent those constraints were. We obtain a general statement of the connection between the density profile and core images: the mean core image magnification  $\langle \mu_{\text{core}} \rangle$  is inversely related to the density at the lensing critical radius  $R_{\text{rad}}$  (eq. 13); and this critical radius is determined by the shape of the density profile (eq. 14), with more concentrated galaxies corresponding to smaller critical radii and fainter core images. Unfortunately, neither our general formalism nor our Nuker law lenses suggest any simple, model independent measure of the mass concentration that determines the core image properties. The interpretation of core image data will therefore con-

tinue to rely on detailed models of individual lenses. The model dependence can be held in check, though, by using general models like the Nuker law or the cuspy lenses introduced by Muñoz et al. (2001), as opposed to overly simple flat core or pure power law models.

We conclude that in many cases the stellar mass in lens galaxies is probably concentrated enough to render core images faint (also see Evans & Hunter 2002). This is not to say that bright core images cannot exist — certainly there are realistic galaxies that predict bright core images, and the probability that they are selected for lensing is non-zero. But the fact that core images have not yet been found (with perhaps one or two exceptions) is probably not a surprise. As the search continues, two-image lenses should be better targets than four-image lenses for revealing core images.

I am very grateful to Marijn Franx for discussions that contributed to the birth and development of this project. I also thank Martin Norbury for interesting discussions and for providing data in advance of publication. This work was supported by NASA through Hubble Fellowship grant HST-HF-01141.01-A from the Space Telescope Science Institute, which is operated by the Association of Universities for Research in Astronomy, Inc., under NASA contract NAS5-26555.

TABLE 1  
GALAXY SAMPLE

(1) Name	(2) $D$ (Mpc)	(3) $\sigma$ (km/s)	(4) $\alpha$	(5) $\beta$	(6) $\gamma$	(7) $\log \kappa_b$	(8) $\log r_b$ (arcsec)	(9) $\log R_{\text{ein}}$ (arcsec)	(10) $\log R_{\text{rad}}$ (arcsec)	(11) $\log \langle \mu_{\text{core}} \rangle$	(12) $\log \langle \mu_{\text{core}} \rangle$	(13) $\log \langle \mu_{\text{core}} \rangle$	(14) Ref
NGC221	0.9	85	0.98	1.36	0.01	2.86	-4.02	-1.26	-3.17	-4.67	-6.00	-6.00	1
	0.7	77	4.66	1.26	0.50	2.56	-3.71	-1.29	-3.28	-4.74	-6.00	-5.31	2
NGC224	0.9	220	4.72	0.87	0.12	3.25	-3.65	0.43	-0.58	-1.65	-1.66	-1.66	1
NGC474	32.5	169	1.23	1.90	0.37	0.91	-1.39	-0.43	-1.30	-2.08	-2.10	-2.10	2
NGC524	24.6	275	1.29	1.00	0.00	1.96	-2.21	0.29	-0.85	-2.13	-2.18	-2.21	1
	32.1	242	0.68	1.69	0.03	1.26	-1.41	-0.02	-0.98	-2.12	-2.15	-2.16	2
NGC596	22.6	165	0.76	1.97	0.55	0.62	-1.20	-0.43	-1.44	-2.31	-2.37	-2.36	1
NGC720	24.1	250	2.32	1.66	0.06	1.12	-1.21	-0.07	-0.90	-1.97	-1.99	-1.99	1
NGC821	23.2	207	1.00	1.59	0.64	1.31	-1.66	-0.34	-1.60	-3.03	-3.20	-3.23	2
NGC1023	10.9	217	4.72	1.18	0.78	1.52	-1.80	-0.16	-1.52	-2.99	-3.11	-3.14	1
NGC1052	17.8	222	1.05	1.43	0.11	1.94	-2.22	-0.26	-1.58	-3.15	-3.28	-3.32	2
NGC1172	31.8	113	1.52	1.64	1.01	0.18	-1.21	-0.76	-6.00	-6.00	-6.00	-6.00	1
NGC1316	19.1	240	1.16	1.00	0.00	1.85	-2.21	0.20	-0.87	-1.96	-1.99	-2.01	1
NGC1399	19.1	333	1.50	1.68	0.07	1.49	-1.33	0.10	-0.95	-2.66	-2.69	-2.72	1
NGC1400	22.9	265	1.39	1.32	0.00	2.08	-2.22	-0.09	-1.49	-3.29	-3.44	-3.52	1
NGC1426	22.9	150	3.62	1.35	0.85	0.89	-1.53	-0.51	-1.52	-2.25	-2.31	-2.30	1
NGC1600	53.5	340	1.98	1.50	0.08	1.02	-0.88	0.26	-0.52	-1.68	-1.69	-1.70	1
NGC1700	37.9	230	0.90	1.30	0.00	2.23	-2.57	-0.19	-1.62	-3.27	-3.51	-3.59	1
	54.1	230	0.46	1.65	0.01	1.80	-2.08	-0.17	-1.40	-2.80	-2.93	-2.96	3V
	54.1	230	0.47	1.68	0.01	1.81	-2.08	-0.19	-1.44	-2.89	-3.03	-3.07	3I
NGC2636	35.7	85	1.84	1.14	0.04	1.41	-2.59	-0.88	-1.87	-1.97	-2.01	-1.99	1
NGC2685	16.2	114	1.69	1.52	0.73	0.64	-1.48	-0.68	-1.56	-1.87	-1.90	-1.89	2
NGC2832	96.2	330	1.84	1.40	0.02	1.27	-1.16	0.23	-0.68	-2.02	-2.04	-2.06	1
NGC2841	14.1	229	0.93	1.02	0.01	2.35	-2.84	0.08	-1.17	-2.41	-2.53	-2.56	1
NGC3115	9.0	280	1.47	1.43	0.78	1.60	-1.69	-0.13	-1.61	-3.59	-4.18	-6.00	1
	6.7	264	1.13	1.80	0.73	1.36	-1.51	-0.25	-1.65	-3.62	-4.00	-6.00	2
NGC3377	10.6	152	1.92	1.33	0.29	2.53	-3.12	-0.74	-2.57	-4.48	-6.00	-6.00	1
NGC3379	10.6	225	1.59	1.43	0.18	1.61	-1.84	-0.21	-1.35	-2.72	-2.78	-2.80	1
	8.1	209	1.82	1.45	0.18	1.71	-1.96	-0.29	-1.50	-2.95	-3.02	-3.03	2
NGC3384	8.1	170	5.36	1.58	0.64	1.35	-1.78	-0.52	-1.61	-2.80	-2.84	-2.84	2
NGC3599	21.7	80	13.01	1.66	0.79	0.50	-1.64	-1.01	-1.65	-1.34	-1.35	-1.34	1
NGC3605	21.7	103	9.14	1.26	0.67	0.92	-1.82	-0.75	-1.64	-1.84	-1.86	-1.85	1
NGC3608	21.7	195	1.05	1.33	0.00	1.88	-2.32	-0.29	-1.53	-2.80	-2.90	-2.91	1
	13.6	195	0.72	1.58	0.00	1.88	-2.28	-0.37	-1.63	-3.03	-3.15	-3.16	3V
	13.6	195	0.78	1.57	0.00	1.92	-2.32	-0.39	-1.67	-3.11	-3.25	-3.26	3I
NGC3900	29.4	118	0.29	1.66	0.51	1.39	-2.24	-1.75	-2.37	-3.65	-6.00	-6.00	2
NGC4026	17.0	195	0.88	1.50	0.68	1.51	-1.92	-0.41	-1.84	-3.41	-3.94	-4.07	2
NGC4143	17.0	270	1.26	2.18	0.59	1.20	-1.35	-0.26	-1.45	-3.23	-3.35	-3.42	2
NGC4150	9.7	85	1.23	1.67	0.58	1.18	-2.28	-1.09	-2.20	-2.69	-2.79	-2.74	2
NGC4168	38.8	185	0.95	1.50	0.14	0.76	-1.11	-0.10	-0.82	-1.24	-1.25	-1.25	1
NGC4239	16.3	60	14.53	0.96	0.65	0.39	-1.78	-1.09	-1.71	-0.75	-0.76	-0.75	1
NGC4261	35.1	326	2.38	1.43	0.00	1.43	-1.32	0.15	-0.86	-2.38	-2.41	-2.44	2
NGC4278	9.7	250	1.63	1.39	0.02	1.96	-2.10	-0.16	-1.50	-3.25	-3.36	-3.40	2
	9.7	250	1.45	1.32	0.00	1.98	-2.13	-0.09	-1.43	-3.12	-3.23	-3.27	3V
	9.7	250	1.25	1.46	0.00	1.90	-2.04	-0.15	-1.43	-3.13	-3.22	-3.25	3I
NGC4291	29.4	278	2.07	1.48	0.02	1.89	-1.92	-0.14	-1.44	-3.28	-3.38	-3.43	2
NGC4365	23.5	262	2.06	1.27	0.15	1.43	-1.51	0.07	-0.96	-2.25	-2.28	-2.30	1
	13.8	262	1.67	1.46	0.11	1.58	-1.63	-0.04	-1.15	-2.66	-2.71	-2.73	3V
	13.8	262	1.52	1.49	0.04	1.61	-1.67	-0.06	-1.17	-2.69	-2.73	-2.75	3I
NGC4374	16.8	296	2.15	1.50	0.13	1.53	-1.47	0.03	-1.05	-2.66	-2.70	-2.72	2
NGC4387	16.3	105	3.36	1.59	0.72	0.38	-1.24	-0.66	-1.33	-1.24	-1.26	-1.25	1
NGC4406	16.8	250	3.31	1.16	0.00	1.70	-1.84	0.03	-1.19	-2.61	-2.67	-2.69	2
	13.8	250	4.13	1.05	0.04	1.80	-1.95	0.13	-1.12	-2.51	-2.58	-2.61	3V
	13.8	250	3.32	1.07	0.00	1.81	-1.97	0.12	-1.14	-2.55	-2.63	-2.66	3I
NGC4417	16.8	84	0.87	1.77	0.71	0.10	-1.28	-0.90	-1.80	-1.75	-1.80	-1.78	2
NGC4434	16.3	115	0.98	1.78	0.70	0.60	-1.51	-0.74	-1.77	-2.31	-2.39	-2.35	1
NGC4458	16.3	105	5.26	1.43	0.49	2.02	-2.81	-0.99	-2.51	-3.87	-4.04	-3.96	1
NGC4464	16.3	125	1.64	1.68	0.88	0.96	-1.81	-0.81	-2.08	-3.11	-6.00	-3.35	1
NGC4467	16.3	72	7.52	2.13	0.98	0.02	-1.38	-1.10	-2.75	-3.38	-6.00	-6.00	1
NGC4472	16.3	300	2.08	1.17	0.04	1.51	-1.51	0.24	-0.82	-2.21	-2.24	-2.26	1
	16.8	303	1.89	1.29	0.04	1.48	-1.42	0.20	-0.84	-2.29	-2.32	-2.34	2
NGC4478	16.3	135	3.32	0.84	0.43	1.75	-2.66	-0.24	-1.17	-1.39	-1.42	-1.42	1
NGC4486	16.3	360	2.82	1.39	0.25	1.32	-1.01	0.36	-0.63	-2.28	-2.29	-2.31	1
NGC4486B	16.3	200	2.78	1.33	0.14	2.24	-2.63	-0.50	-2.10	-3.90	-4.33	-4.38	1
NGC4551	16.3	121	2.94	1.23	0.80	0.54	-1.30	-0.52	-1.36	-1.56	-1.59	-1.58	1
NGC4552	16.3	260	1.48	1.30	0.00	1.93	-2.08	-0.05	-1.36	-3.02	-3.12	-3.16	1
	13.8	260	2.17	1.06	0.00	2.06	-2.25	0.14	-1.23	-2.79	-2.92	-2.98	3V
	13.8	260	2.10	1.08	0.04	2.06	-2.23	0.12	-1.27	-2.87	-3.00	-3.06	3I
NGC4564	16.3	165	0.25	1.90	0.05	1.61	-2.17	-0.45	-1.80	-3.02	-3.33	-3.29	1
NGC4570	16.3	195	3.72	1.49	0.85	1.04	-1.44	-0.36	-1.43	-2.57	-2.65	-2.65	1
NGC4589	30.0	228	1.09	1.18	0.11	1.93	-2.27	-0.07	-1.32	-2.64	-2.75	-2.77	2
	24.4	228	0.43	1.62	0.00	1.55	-1.80	-0.05	-1.12	-2.30	-2.35	-2.36	3V
	24.4	228	0.50	1.58	0.01	1.68	-1.95	-0.11	-1.24	-2.50	-2.58	-2.59	3I
NGC4621	16.3	250	0.19	1.71	0.50	1.16	-1.42	-0.10	-1.90	-3.94	-6.00	-6.00	1
NGC4636	16.3	210	1.64	1.33	0.13	1.14	-1.38	-0.04	-0.90	-1.77	-1.78	-1.78	1
	17.0	207	1.69	1.56	0.13	1.07	-1.30	-0.14	-0.96	-1.84	-1.85	-1.85	2
NGC4649	16.3	360	2.00	1.30	0.15	1.55	-1.34	0.32	-0.79	-2.50	-2.54	-2.57	1
NGC4697	11.2	175	24.86	1.04	0.74	1.27	-1.64	-0.11	-1.26	-2.24	-2.28	-2.28	1
NGC4742	13.3	105	48.60	1.99	1.09	0.78	-1.83	-1.05	-6.00	-6.00	-6.00	-6.00	1

## REFERENCES

- Barnes, J. E., & Hernquist, L. 1992, *ARA&A*, 30, 705  
 Blandford, R. D., & Kochanek, C. S. 1987, *ApJ*, 321, 658  
 Blumenthal, G. R., Faber, S. M., Flores, R., & Primack, J. R. 1986, *ApJ*, 330, 27  
 Burke, W. L. 1981, *ApJ*, 244, L1  
 Byun, Y.-I., et al. 1996, *AJ*, 111, 1889  
 Carollo, C. M., Franx, M., Illingworth, G. D., & Forbes, D. A. 1997, *ApJ*, 481, 710  
 Carollo, C. M., & Stiavelli, M. 1998, *AJ*, 115, 2306  
 Chen, G. H., & Hewitt, J. N. 1993, *AJ*, 106, 1719  
 de Zeeuw, T., & Franx, M. 1991, *ARA&A*, 29, 239  
 Ebisuzaki, T., Makino, J., & Okumura, S. K. 1991, *Nature*, 354, 212  
 Egami, E., Neugebauer, G., Soifer, B. T., Matthews, K., Ressler, M., Becklin, E. E., Murphy, T. W., & Dale, D. A. 2000, *ApJ*, 535, 561  
 Evans, N. W., & Hunter, C. 2002, preprint (astro-ph/0204206)  
 Faber, S., et al. 1997, *AJ*, 114, 1771  
 Gebhardt, K., et al. 2000, *ApJ*, 539, L13  
 Gerhard, O., Kronawitter, A., Saglia, R. P., & Bender, R. 2001, *AJ*, 121, 1936  
 Hernquist, L. 1990, *ApJ*, 356, 359  
 Hinshaw, G., & Krauss, L. M. 1987, *ApJ*, 320, 468  
 Ibata, R. A., Lewis, G. F., Irwin, M. J., Lehár, J., & Totten, E. J. 1999, *AJ*, 118, 1922  
 Kayser, R., Refsdal, S., & Stabell, R. 1986, *A&A*, 166, 36  
 Keeton, C. R. 2001, *ApJ*, 561, 46  
 Kochanek, C. S. 1996, *ApJ*, 466, 638  
 Kochanek, C. S., Falco, E. E., Impey, C. D., Lehár, J., McLeod, B. A., Rix, H.-W., Keeton, C. R., Muñoz, J. A., & Peng, C. Y. 2000, *ApJ*, 543, 131  
 Lauer, T. R., et al. 1995, *AJ*, 110, 2622  
 Lewis, G., Carilli, C., Papadopoulos, P., & Ivison, R. J. 2002, *MNRAS*, 330, L15  
 Magorrian, J., et al. 1998, *AJ*, 115, 2285  
 Mao, S., Witt, H. J., & Koopmans, L. V. E. 2001, *MNRAS*, 323, 301  
 Mellier, Y., Fort, B., & Kneib, J.-P. 1993, *ApJ*, 407, 33  
 Merritt, D., & Ferrarese, L. 2001, *ApJ*, 547, 140  
 Milosavljevic, M., & Merritt, D. 2001, *ApJ*, 563, 34  
 Milosavljevic, M., Merritt, D., Rest, A., & van den Bosch, F. C. 2001, preprint (astro-ph/0110185)  
 Molikawa, K., & Hattori, M. 2001, *ApJ*, 559, 544  
 Muñoz, J. A., Kochanek, C. S., & Keeton, C. R. 2001, *ApJ*, 558, 657  
 Narasimha, D., Subramanian, K., & Chitre, S. M. 1986, *Nature*, 321, 45  
 Narayan, R., Blandford, R., & Nityananda, R. 1984, *Nature*, 310, 112  
 Narayan, R., & Schneider, P. 1990, *MNRAS*, 243, 192  
 Norbury, M. A., Rusin, D., Jackson, N., Browne, I. W. A., & Wilkinson, P. N. 2002, *MNRAS*, submitted  
 Oguri, M., Taruya, A., & Suto, Y. 2001, *ApJ*, 559, 572  
 Ravindranath, S., Ho, L. C., Peng, C. Y., Filippenko, A. V., & Sargent, W. L. W. 2001, *AJ*, 122, 653  
 Rest, A., van den Bosch, F. C., Jaffe, W., Tran, H., Tsvetanov, Z., Ford, H. C., Davies, J., & Schafer, J. 2001, *AJ*, 121, 2431  
 Rusin, D., et al. 2001, *ApJ*, 557, 594  
 Rusin, D., & Ma, C.-P. 2001, *ApJ*, 549, L33  
 Schneider, P., Ehlers, J., & Falco, E. E. 1992, *Gravitational Lenses* (New York: Springer)  
 Schramm, T. 1990, *A&A*, 231, 19  
 Smail, I., Dressler, A., Kneib, J.-P., Ellis, R. S., Couch, W. J., Sharples, R. M., & Oemler, A. 1996, *ApJ*, 469, 508  
 Spergel, D. N., & Steinhardt, P. J. 2000, *Phys. Rev. Lett.*, 84, 3760  
 Tremaine, S. 1997, in *Unsolved Problems in Astrophysics*, ed. J. N. Bahcall & J. P. Ostriker (Princeton: Princeton Univ. Press), 137  
 Treu, T., & Koopmans, L. V. E. 2002, preprint (astro-ph/0202342)  
 Wallington, S., & Narayan, R. 1993, *ApJ*, 403, 517  
 Wambsgans, J. 1997, *MNRAS*, 284, 172  
 Winn, J. N., Morgan, N. D., Hewitt, J. N., Kochanek, C. S., Lovell, J. E. J., Patnaik, A. R., Pindor, B., Schechter, P. L., & Schommer, R. A. 2002, *AJ*, 123, 10

TABLE 1—*Continued*

(1) Name	(2) $D$ (Mpc)	(3) $\sigma$ (km/s)	(4) $\alpha$	(5) $\beta$	(6) $\gamma$	(7) $\log \kappa_b$	(8) $\log r_b$ (arcsec)	(9) $\log R_{\text{ein}}$ (arcsec)	(10) $\log R_{\text{rad}}$ (arcsec)	(11) $\log(\mu_{\text{core}})$	(12) $\log(\mu_{\text{core}})$	(13) $\log(\mu_{\text{core}})$	(14) Ref
NGC4874	99.5	290	2.33	1.37	0.13	0.71	-0.68	0.25	-0.39	-1.08	-1.08	-1.09	1
NGC4889	99.5	350	2.61	1.35	0.05	1.06	-0.88	0.33	-0.47	-1.66	-1.68	-1.69	1
NGC5273	21.3	52	7.03	1.32	0.37	0.48	-1.93	-1.26	-1.79	-0.72	-0.73	-0.73	2
NGC5813	30.2	225	2.15	1.33	0.08	1.50	-1.72	-0.13	-1.19	-2.42	-2.46	-2.47	1
	21.2	225	1.77	1.41	0.03	1.57	-1.79	-0.17	-1.27	-2.58	-2.62	-2.63	3V
	21.2	225	1.67	1.46	0.01	1.58	-1.80	-0.20	-1.29	-2.62	-2.67	-2.68	3I
NGC5838	28.5	290	2.57	1.87	0.93	0.83	-0.98	-0.12	-1.29	-2.97	-6.00	-6.00	2
NGC5845	30.1	260	1.27	2.74	0.51	1.03	-1.27	-0.35	-1.44	-3.14	-3.23	-3.27	1
NGC5982	38.7	256	1.73	1.28	0.06	1.65	-1.80	-0.02	-1.16	-2.57	-2.62	-2.65	2
	39.9	256	2.15	1.19	0.12	1.64	-1.79	0.03	-1.13	-2.50	-2.55	-2.58	3V
	39.9	256	2.17	1.19	0.12	1.64	-1.80	0.03	-1.13	-2.51	-2.57	-2.59	3I
NGC6166	120.0	300	3.32	0.99	0.08	0.67	-0.68	0.35	-0.27	-0.74	-0.75	-0.76	1
NGC6340	22.0	137	2.46	1.28	0.59	1.61	-2.28	-0.62	-1.91	-2.97	-3.09	-3.06	2
	18.0	137	1.73	1.24	0.72	1.38	-2.08	-0.57	-1.80	-2.70	-2.83	-2.79	4
NGC7332	21.7	130	4.25	1.34	0.90	1.12	-1.88	-0.68	-1.87	-2.76	-2.93	-2.86	1
NGC7457	12.3	77	2.32	1.03	0.35	1.22	-2.46	-0.90	-1.83	-1.67	-1.71	-1.69	2
NGC7626	45.3	273	1.84	1.30	0.36	1.57	-1.64	0.01	-1.15	-2.65	-2.71	-2.75	2
	49.5	273	1.53	1.23	0.00	1.64	-1.77	0.08	-1.03	-2.40	-2.45	-2.47	3V
	49.5	273	1.29	1.27	0.00	1.65	-1.78	0.07	-1.04	-2.42	-2.47	-2.49	3I
NGC7743	24.4	85	5.36	1.38	0.50	1.47	-2.48	-1.04	-2.19	-2.76	-2.82	-2.79	2
NGC7768	110.0	290	1.92	1.21	0.00	1.39	-1.46	0.17	-0.82	-2.04	-2.07	-2.08	1

Note. — Col. 2: Distance (assuming  $H_0 = 75 \text{ km s}^{-1} \text{ Mpc}^{-1}$ ). Col. 3: Central stellar velocity dispersion. Cols. 4-6: Fitted Nuker law parameters. Cols. 7-10: Logarithms of the lensing strength  $\kappa_b$ , break radius  $r_b$ , Einstein radius  $R_{\text{ein}}$ , and radial critical radius  $R_{\text{rad}}$ . Note that if any quantity is zero, we arbitrarily set its logarithm to  $-6$ . Col. 11: Logarithm of mean core image magnification for the Nuker law lens. Cols. 12-13: Logarithm of mean core image magnification for the Nuker law lens plus a supermassive black hole normalized by the  $M_\bullet$ - $\sigma$  correlations of Gebhardt et al. (2000) and Merritt & Ferrarese (2001), respectively. Col. 14: References as follows: (1) Faber et al. (1997); (2) Ravindranath et al. (2001); (3V) and (3I) V and I band samples, respectively, from Carollo et al. (1997); (4) Carollo & Stiavelli (1998).